Lawrence Berkeley National Laboratory
Recent Work

Title
AC Calorimeter for Measurements of Adsorbed Gases on Metal Films at {sup 4}He Temperatures

Permalink
https://escholarship.org/uc/item/65v2d5w3

Journal
Review of scientific instruments, 61(2)

Authors
Kenny, T.W.
Richards, P.L.

Publication Date
1989-07-01

Lawrence Berkeley Laboratory

UNIVERSITY OF CALIFORNIA

Materials & Chemical Sciences Division

AC Calorimeter for Measurements of Adsorbed Gases on Metal Films at ^{4}He Temperatures

T.W. Kenny and P.L. Richards

July 1989

DISCLAIMER

AC calorimeter for measurements of adsorbed gases on metal films at ^{4}He temperatures.

T. W. Kenny* and P. L. Richards

Department of Physics, University of California

and Materials and Chemical Sciences Division,

Lawrence Berkeley Laboratory

Berkeley, California 94720

Abstract

An analysis is presented of the performance of an ideal ac calorimeter limited only by thermodynamic noise. A calorimeter based on this analysis is described which is designed for studies of the heat capacity of monolayers and multilayers of atoms and molecules adsorbed on a variety of surfaces. The calorimeter consists of Ge:Ga thermometers and NiCr heaters mounted on one side of a sapphire substrate, with an evaporated film deposited on the other side. The calorimeter is mounted on a ^{4}He cold finger in a UHV system allowing heat capacity measurements down to 1.6 K. In order to verify the performance of the calorimeter, measurements have been made of the heat capacity of 25 μg samples of indium, and of submonolayer coverages of ^{4}He on sapphire. The measured sensitivity corresponds to $<10^{-2}$ monolayers of ^{4}He adsorbed on the surface of the calorimeter in the gas phase.

PACS No 67.70

Introduction

The thermodynamics of two-dimensional systems have received much attention since the discovery of anomalies in the heat capacity of adsorbed layers of ^{4}He on graphite.[1] Measurements of the heat capacity of adsorbed monolayers have generally been limited to substrates which provide large surface area per unit volume: Exfoliated graphite, MgO smoke, vycor, and mylar are examples of such substrates. Of these, exfoliated graphite is the most widely used. Measured phase diagrams of monolayers of helium and other noble gases adsorbed on these substrates have revealed a wide variety of phenomena, including the formation of solid phases commensurate with the substrate crystalline structure.[2-6] It is clear that the observed commensurate phases are not intrinsic to two dimensional systems, but are influenced by interactions with the crystalline substrate. A number of sophisticated theoretical models have been constructed to describe the behavior of these systems.[7-13] The interaction between the adsorbate and the substrate has also been thoroughly characterized.[14-16] Particular attention has been paid to the lateral corrugation of the physisorption potential which arises from the crystallinity of the substrates.[15,16] Successful theoretical descriptions of some of these systems have entirely neglected the adsorbate-adsorbate interactions in favor of adsorbate-substrate interactions.[17,18]

Metallic substrates present a much smaller corrugation in the physisorption potential for noble gases and should be considerably less complicated from a theoretical standpoint.[19] However, well-characterized metallic substrates have not been available with sufficiently large surface area and low enough heat capacity for measurements of the type carried

out on exfoliated graphite. We have designed a novel ac microcalorimeter for the studies of noble gases adsorbed on metals. The substrate for adsorption is an evaporated film which has been deposited on optically polished sapphire. The film can be composed of any material suitable for UHV evaporation. For example, thin Ag films deposited on sapphire have been studied by scanning tunneling microscopy, and have been shown to be highly uniform.[20] The ability to study the heat capacity of adsorbates on a wide variety of substrates should help us distinguish fundamental two-dimensional behavior from substrate-induced behavior.

The use of ac microcalorimetry imposes limitations on the studies of adsorbed gases. Adsorbed layers with vapor pressures above $\sim 10^{-7}$ torr cannot be studied because the thermal conductance of the gas would be significant compared with the $\sim 10^{-6}$ W/K thermal conductance between the calorimeter and the heat sink. Since less than 1% of the cold surface area of the apparatus is part of the calorimeter, it is not possible to deduce the coverage on the calorimeter from the amount of ^{4}He remaining in the 3-D gas phase after exposure. Consequently, adsorption isotherms, which are useful for the characterization of conventional surface calorimeters, cannot be measured. Despite these limitations, the ability to do heat capacity measurements on a variety of substrates, including metals, should prove very valuable.

In this report, we present a calculation of the contributions of fundamental noise sources to the measured signal of an ideal ac calorimeter. These results are used to select parameters for a practical calorimeter. The apparatus, the electronics, and the computer data

acquisition system are then described. We then present measurements of the heat capacity of 25 μg samples of indium, and measurements of ^{4}He adsorbed on the sapphire substrate to demonstrate the accuracy and sensitivity of the instrument.

I. Analysis of the Calorimeter

The technique chosen for heat capacity measurements depends on the intrinsic time constants of the calorimeter. For calorimeters constructed with exfoliated graphite or other porous adsorption media, the internal thermal time constants can be 10^2 to 10^3 seconds. For this reason, the heat capacity of many adsorbed monolayer systems has been measured by slow adiabatic techniques.

In our experiment, the heat capacity of the calorimeter is made very small so that the contribution of the adsorbate can be detected. At the same time, the thermal conductance to the heat sink must be large enough to allow measurements near the minimum operating temperature of the cryostat. The resulting thermal time constant of our calorimeter is between 1 s and 10^{-3} s, and is appropriate for ac calorimetry.[21]

In order to optimize the measurement, we consider an ideal calorimeter with heat capacity C isolated from a heat sink at temperature T_0 by a thermal conductance G. The calorimeter has a calibrated thermometer with resistance R(T) and a heater with resistance R_H. It is assumed that the internal time constants of all elements of the calorimeter including the thermometers are much shorter than C/G.

4

Under normal operating conditions, the thermometer is biased with a dc current $I = V_{dc}/R_T$, and the heaters are biased with an ac voltage V_H at frequency $\omega/2$. The temperature of the calorimeter oscillates at the frequency ω with amplitude

$$T_{ac} = \frac{V_H^2}{2\ R_H\ [(\omega C)^2 + (G)^2]^{1/2}} \ .$$

(1)

Due to the temperature dependence of the resistance, the voltage across the thermometer oscillates with amplitude $V_{ac} = V_{dc}\alpha T_{ac}$ where α is defined as $\partial Log(R_T)/\partial T$. When $\omega C/G \gg 1$, the heat capacity can be deduced from a measurement of V_{ac}.

We can calculate the errors induced in the measured signal from fundamental noise sources. Johnson noise in the thermometer has a spectral density[22]

$$(V_J)^2 = 4\ k_B\ R_T\ T\ ,$$

(2)

where k_B is Boltzmann's constant.

Energy fluctuations also contribute to the noise in a calorimeter. These arise from the statistical fluctuations in the rate of arrival of phonons at the heat sink and are also known as phonon noise.[23] Because of the temperature dependence of the resistance of the thermometer, these fluctuations contribute to the voltage noise. The resulting voltage fluctuations have a spectral density

5

$$(V_P)^2 = \frac{4\ k_B\ T^2\ G\ (V_{dc}\ \alpha)^2}{(\omega C)^2 + (G)^2}\ . \tag{3}$$

The voltage fluctuations (2) and (3) are statistically independent and their spectral densities are additive. The ratio of noise voltage to signal voltage is

$$\frac{V_N^2}{V_{ac}^2} = \frac{16 k_B T \Delta F R_H^2 [(\omega C)^2 + (G)^2]}{V_{dc}^2\ \alpha^2\ V_H^4}\left[R_T + \frac{GTV_{dc}^2\alpha^2}{(\omega C)^2 + (G)^2}\right], \tag{4}$$

where ΔF is the bandwidth of the measurement.

To optimize the sensitivity of an ac calorimeter, the ratio of noise to signal is minimized subject to two experimental constraints:

1) The maximum permissible amplitude of the oscillation, T_{ac}, which sets the temperature resolution, is determined by the experiment to be done. This constraint is introduced by replacing $((\omega C)^2 + (G)^2)$ in Eq. 4 with $(V_H^2/2T_{ac}R_H)^2$. This leaves the ratio (4) in the form

$$\frac{V_N^2}{V_{ac}^2} = 4\ k_B\ T\left(\frac{R_T}{V_{dc}^2\ \alpha^2\ T_{ac}^2} + \frac{4\ G\ T\ R_H^2}{V_H^4}\right)\ . \tag{5}$$

2) The temperature of the calorimeter is also specified by the measurement to be done. Therefore, the minimum difference in temperature between the calorimeter and the heat sink determines the

6

maximum total measurement bias power in terms of the thermal conductance to the heat sink.

$$(T-T_0) = \frac{V_H^2}{2R_HG} + \frac{V_{dc}^2}{R_TG} = \Delta T_H + \Delta T_B. \qquad (6)$$

Here, $\Delta T_H = V_H^2/2R_HG$ is the time average temperature rise due to the ac bias on the heater, and $\Delta T_B = V_{dc}^2/R_TG$ is the temperature rise due to the dc bias on the thermometer. With these substitutions, Eq. 4 takes the form

$$\frac{V_N^2}{V_{ac}^2} = \frac{4\,k_B\,T}{G}\left(\frac{1}{\alpha^2\,T_{ac}^2\,\Delta T_B} + \frac{T}{\Delta T_H^2}\right). \qquad (7)$$

Of the terms in the parentheses, only ΔT_B, ΔT_H, and α can be freely adjusted. The other terms in the parentheses are determined prior to the measurement. In principle, one can improve the sensitivity at a particular temperature by choosing thermometers with very large α. However, rapid variations in the resistance of the thermometer with temperature can make measurements over a broad temperature range exceedingly difficult. In practice, values of α of order 1 K^{-1} provide a compromise between sensitivity and versatility.

Given values of T, T_{ac}, and α, the expression in the parentheses can easily be minimized subject to the constraint of Eq. 6. The appearance of G in the denominator of Eq. 7 indicates that the noise in an ideal calorimeter can be reduced arbitrarily by increasing G. For non-ideal calorimeters, however, the limits imposed by internal time constants within the calorimeter must be considered. As Eq. 1 shows, when G is increased,

7

V_{ac} becomes independent of C unless ω is also increased. Internal time constants in real calorimeters set a limit to the highest frequencies at which Eq. 1 can be used. Internal time constants can arise from electrical RC effects, or thermal relaxation within the elements of the calorimeter. A much more detailed thermal analysis would be required to interpret data at frequencies comparable to the inverse of the internal time constants.

Further limits to the sensitivity of an ac calorimeter are imposed by the accuracy of the devices which record the electronic signals from the experiment. At present, 16-bit A-D converters are commercially available for most computers, and 18-bit devices are starting to become available.

Finally, the presence of slow thermal drifts can reduce the accuracy of measurements that depend on the difference between heat capacities measured at different times. Because of the strong temperature dependence of the heat capacity of the calorimeter, variations in the temperature of the calorimeter will appear as large variations in signal. As a result, active thermal regulation of the calorimeter is necessary. The accuracy and stability of the regulation scheme must be optimized to minimize its contribution to measurement noise.

In summary, we have seen that the sensitivity of an ideal calorimeter can be arbitrarily increased. Practical limits to the sensitivity are imposed, however, by the internal time constants of the calorimeter, the accuracy of the ADC, and the stability of the thermal regulation. For the calorimeters described in this report, it is usually the case that for operation at frequencies just below the internal relaxation frequencies, the sensitivity is

8

limited by the accuracy of the thermal regulation. Nevertheless, enough sensitivity has been obtained to detect a small fraction of a monolayer of ^{4}He adsorbed on the metallic surface of the calorimeter.[24]

II Experimental Apparatus and Procedure
A. Calorimeter

The design of the calorimeter used in these experiments is based on that of a composite bolometer which is the most sensitive available direct detector of far-infrared radiation.[25] A bolometer operates by measuring the temperature rise induced by the absorption of radiation. In attempting to improve the sensitivity of composite bolometers, workers have developed resistance thermometers with low noise, low heat capacity, and high sensitivity. These advances have been incorporated directly into the design of the microcalorimeters described in this report. A composite bolometer can be converted to a calorimeter by attaching a resistive heater. The heat capacity can then be calculated from the absorbed power and the temperature rise.

A drawing of the calorimeter is shown in Fig. 1. The calorimeter is constructed on a 125 μm sapphire substrate which has been optically polished on one surface. The use of thinner substrates would provide more sensitivity, but would make the calorimeters more fragile. Sapphire has been chosen as the substrate material because of its small heat capacity at ^{4}He temperatures. A pair of commercially available NiCr films deposited on Si wafers serve as resistive heaters.[26] Six leads of 25μm diameter Cu wire, two thermometers and two heater packages are attached to the substrate with an Ag-filled conductive epoxy.[27] The Cu leads provide the

9

thermal conductance to the heat sinks. Two heaters are required; one is used to apply the ac power, and the other is used to actively regulate the average temperature of the calorimeter. In principle, a single heater could be ac and dc biased simultaneously. This can complicate the measurement, because it would induce an oscillation at half the measurement frequency, whose amplitude depended on the regulation current. Because of nonlinearities in the thermometer resistance, as well as electrical cross-talk, some distortion of the signal at the measurement frequency might result. For this reason, two separate heaters are used.

The thermometers are made from ultrapure single crystal Ge which has been doped with Ga acceptors by neutron transmutation (NTD). The preparation of these thermometers is described elsewhere.[28] Thermometers as small as $(100\mu m)^3$ have been fabricated with resistances that are compatible with the current and voltage noise of commercially available preamplifiers. They are useful in this application because of their low heat capacity and large α. Electrical contacts which contribute no excess noise are made by B^+-ion implantation and Cr/Au metallization.

Despite their many advantages, some properties of these thermometers cause difficulties with the measurement.[29] The dominant conduction mechanism at ^{4}He temperatures is variable-range hopping. This mechanism has been carefully studied, both experimentally and theoretically. The resistance is a function of both the temperature and the applied electric field. Because of the field dependence, resistivity measurements must be made with either very small electric fields, or exactly the same fields as used for calibration. Time constants in excess of

10^{-2} s due to weak electron-phonon coupling have also been observed in variable range hopping systems.[30,31] Experiments on NTD Ge doped to 10^{16} cm^{-3}, however, have shown no evidence for internal time constants at frequencies as high as 10^3 Hz. In addition, the electric field effects are less significant in more heavily doped thermometers, as less voltage is required to achieve a given bias power. All of these results are discussed at length elsewhere.[31] We have assembled many calorimeters with heavily doped NTD thermometers and, with care, have obtained reliable results.

The thermal time constant of each calorimeter must be measured to verify that, at the measurement frequency, the signal is directly related to the heat capacity. A fixed ac heater bias and dc thermometer bias is applied to the calorimeter. The amplitude and phase of the voltage oscillation of the thermometer is then measured as a function of the frequency of the oscillation and compared with the relation

$$T_{AC} = \frac{P_{AC}}{G + i\omega C} \, , \tag{8}$$

where G is the thermal conductance to the heat sink, and P_{AC} is the amplitude of the applied power oscillation. The product of the amplitude of the voltage oscillation and the frequency of oscillation is plotted as a function of frequency in Fig. 2. In such a plot, the acceptable operating frequencies are on the plateau of the curve. For the figure, the acceptable frequencies are between 300 Hz and 1 kHz. At higher frequencies, additional time constants further steepen the rolloff. For the measurements

reported here, the capacitance of the heat sinks, coupled with the resistance of the thermometers, is responsible for the high-frequency rolloff.

The calorimeter is mounted within an aluminum and stainless steel frame which constrains its motion with negligible thermal contact. The frame also masks the evaporation so that metallic paths from the front surface of the calorimeter to other parts of the apparatus do not exist. This is important because the calorimeter is always warmer than its surroundings, and metallic paths can allow migration of the adsorbed atoms off of the calorimeter during the measurement. The frame is attached to the mount with stainless steel screws. A drawing of the frame and the mount is shown in Fig. 3. After assembly, the calorimeter, frame and mount are submerged in ^{4}He for thermometer calibration. The mount is then attached to the end of the cold finger of the cryostat with stainless steel screws as is shown in Fig. 3. A 12 μm Au foil is placed between the mount and the cold finger to improve thermal contact.

A radiation shield is mounted on the cold finger allowing the calorimeter to be operated at temperatures as low as 1.6 K. The inside of this shield has been coated with colloidal graphite to absorb room-temperature radiation which leaks around the shield and to provide additional pumping of background ^{4}He gas. Further reductions in temperature are only possible with the aid of better refrigeration, such as with ^{3}He.

Low thermal conductance stainless steel coaxial cables are used throughout the apparatus. Electrical leads reach the calorimeter through a

liquid nitrogen temperature feedthrough into the UHV system. Two stages of heat sinks on the mount provide thermal isolation for the calorimeter. The heat sinks are made from 1.5 x 10.0 x .08 mm^3 Cu plates which are attached with Stychast[32] epoxy. This epoxy contains small glass spheres which insure electrical insulation between flat, metallic surfaces while providing good thermal contact.[33]

The calorimeter can be warmed to room temperature with the cold finger held at 1.6 K by passing a dc current through one of the heaters. This step is necessary to anneal metal films and to desorb contaminants.

At ^{4}He temperatures, the heat capacity of the calorimeter is dominated by the sapphire substrate and is proportional to T^3. Deviations from this dependence arise below 2.5 K due to the metallic parts of the calorimeter whose heat capacities have a component proportional to T. The heat capacity of the bare calorimeter is measured as a function of temperature at the beginning of each experiment. After the adsorption of the sample gas, the heat capacity is measured again. Subtraction of the two measurements yields the heat capacity of the adsorbed sample.

B. UHV System and Cryostat

A cross section of the UHV system and cryostat used in this experiment is shown in Fig. 4. The upper half of the apparatus is a stainless steel cryostat which contains chambers for liquid nitrogen and liquid ^{4}He. The cryostat is evacuated by a 40 l/s turbomolecular pump, and is also cryopumped by the surfaces of the storage chambers.

The lower half of the apparatus is a commercial ion-pumped UHV system which can be evacuated to $< 10^{-9}$ torr when at room temperature without bakeout. The outer radiation shields are cooled by conduction from the liquid nitrogen storage chamber in the cryostat. The cold finger is cooled to 1.6 K by direct contact with superfluid ^{4}He which flows down a thin tube from the cryostat. During measurement, the pressure near the sample is less than 10^{-12} torr due to cryopumping on the surrounding radiation shields. A shutter in the nitrogen temperature radiation shields can be rotated to allow the evaporation of a metal film onto the calorimeter substrate. The film thicknesses are monitored by a commercial quartz oscillator near the evaporation filament and are typically of order 1000 Å. During dosing, gas enters a room temperature effusion cell from a stainless steel gas line through a leak valve. The pressure within the effusion cell is monitored by an ion gauge. The dosing flux can be calculated from the pressure, the dimensions of the cell, and the distance to the calorimeter. Since the sticking coefficient is not always known, adsorbate coverages are uncertain, except when they can be deduced from the heat capacity measurement.

Since bakeouts are unnecessary, low melting point materials such as indium can be used between the joints in the radiation shields and in the cold finger. Also, the background pressure in the apparatus is only important during the measurement, when much of it is very cold. This allows the use of many materials on or near the cold finger which are not usually acceptable in UHV systems. For example, epoxies[32] have been used in the construction of heat sinks. Granules of activated charcoal have been attached to the cold finger in several places to improve pumping of

background ^{4}He gas. Conductive epoxies[28] have been used in calorimeter construction. Various infrared absorbers have been used to coat the radiation shields which surround the calorimeter. The ability to use these materials has greatly simplified the design and operation of this experiment.

C. Measurement Electronics

The electronic system used for this measurement can be described in three sections : the ac heater bias, the thermometer bias and readout, and the temperature regulation. A block diagram of the entire measurement circuit is shown in 5.

The ac heater bias is generated by the reference channel of a lock-in amplifier.[34] This source was chosen for its excellent amplitude stability and ease of frequency and amplitude adjustment. The amplitude of the ac bias voltage is measured by the same lock-in amplifier, allowing small amplitude drifts to be removed from the data. This voltage is applied to one of the heaters on the calorimeter and produces a temperature oscillation in the calorimeter.

The dc bias for the thermometer is produced by three 9 V mercury batteries which are connected in series across a 500 kΩ 10-turn wire-wound potentiometer. The center terminal of the potentiometer is attached to a room temperature metal film load resistor in series with the cold thermometer. When used to bias a resistance thermometer whose temperature is oscillating, this stable current produces a voltage with both dc and ac components. The dc component is directly related to the average

temperature of the calorimeter, while the dc component is used to calculate the heat capacity. The voltage of the thermometer is processed by both a dc preamplifier,[35] which is low-pass filtered to remove the voltage oscillation, and by another lock-in amplifier,[36] which uses the ac bias from the the first lock-in as its reference signal.

An LSI-11 computer with an ADC-DAC board[37] is used to record the measured voltages and produce the thermal regulation voltage which is applied to one of the films on the calorimeter. The resolution of the 12-bit DAC on this board is inadequate for the temperature regulation. An effective resolution of 18-bits is obtained by dividing one of the 12-bit DAC channels by 10^2 and adding it to the other. The voltages are generated by separate D-A channels with a common ground, and so neither of the wires leading to this heater can be externally grounded.

The computer program regulates the temperature and collects the data as follows. The total dc bias applied to the load resistor and thermometer is monitored by one channel of the ADC. Another channel monitors the output of the dc preamplifier. The computer program calculates the average resistance of the thermometer from these two voltages, and then calculates the temperature of the calorimeter. The regulation voltage is then adjusted by the computer so as to reduce the difference between the measured temperature and the specified temperature. Once the temperature of the calorimeter has been within 0.02% of the specified temperature for more than 10 lock-in time constants, the computer begins to record the outputs of the two lock-in

amplifiers. The heat capacity is given by the following relationship between the measured quantities:

$$C = \frac{V_{DC} \, \alpha \, V_H^2}{2 \, \omega \, R_H \, V_{AC}} \, .$$

(9)

When the signals have been averaged sufficiently, a new temperature is selected and the process begins again. This continues until the temperature scan is completed. Typically, a 40-point scan takes less than 1/2 hour to complete. This is important, as the experiments are limited to 6 hours by the hold-time of the cryostat.

III Measurements

This apparatus has been used to study many adsorbed systems. In particular, the heat capacity of ^{4}He adsorbed on evaporated Ag films has been investigated over a wide range of coverages and is reported elsewhere.[38] In order to demonstrate the performance of this apparatus, measurements of the heat capacity of small samples of In are presented here.

The calorimeters are often assembled with a small (~25 μg) Indium sample attached to the back surface. These samples are prepared by trimming the edge of a 250 μm foil with a razor blade. They are weighed in a laboratory microbalance with a resolution of less than 5 μg and then attached to the calorimeter with conductive epoxy. Because of the superconducting phase transition in indium, there will be a small discontinuity in the heat capacity of the calorimeter at 3.41 K. The

location and magnitude of the discontinuity is routinely studied in the early stages of the characterization of a new calorimeter to verify the calibration of the thermometers and the operation of the instrument.

Hysteresis in the transitions of type 1 superconductors has been attributed to supercooling below the superconducting transition.[39] There is a positive free energy associated with the creation of boundaries between normal and superconducting phases in the presence of an applied magnetic field. As a result, the normal phase can persist to a temperature below T_c.

Ordinarily, supercooling experiments are carried out by fixing the temperature, applying a magnetic field in excess of the critical field, $H_c(T)$, and then slowly reducing the field until the superconducting transition occurs at H_{appl}. In experiments of this type on single crystals of In near T_c, the limiting value of H_{appl} was found to be [40]

$$\frac{H_{appl}}{H_c(T)} = 0.158 \ .$$
(10)

In our experiments, the temperature is varied in the presence of a fixed applied magnetic field which is due to the magnetic field of the earth and the ion pumps. Magnetometer measurements at several positions around and inside the apparatus indicate an ambient magnetic field of about 0.44 Gauss. The greatest amount of supercooling expected in the presence of such a field is given by:

$$\Delta T_c = T_c \left\{ 1 - \left[1 - \frac{H_{appl}}{0.158 \ H_c(0)} \right]^{1/2} \right\} \ .$$
(11)

The expected upper limit to the supercooling ΔT_C of In is about 17 mK. The energy required to form superconducting-normal boundaries near defects in the crystal can be much less than in a perfect crystal. Such defects can give rise to the formation of boundaries which trigger the phase transition for smaller values of ΔT_C.

Figure 6 shows the heat capacity of the calorimeter in the neighborhood of the expected superconducting transition of In. Measurements made with both increasing and decreasing temperatures are shown. The observed hysteresis indicates a supercooling of about 4 mK, which is well within the limits of ideal supercooling in the presence of the ambient magnetic field. The amplitude of the discontinuity is consistent with that expected for the 25 ± 5 μg of In that was attached to this calorimeter.

The sharp discontinuities in Fig. 6 occur because of the hysteresis in the phase transition. In the absence of hysteresis, the transitions would be broadened by the 1 mK temperature oscillation used in the measurement. Figure 7 shows the heat capacity of another calorimeter with a different In sample. In this case, the hysteresis is absent, and the width of the discontinuity is about 5 mK, which is well in excess of the 1 mK temperature oscillation. The absence of supercooling and the occurrance of a broadened transition in this sample are probably due to a greater concentration of defects which can nucleate the formation of the superconducting phase. The two In samples investigated here probably

differ in the amount and type of crystalline defects, although they were prepared and mounted in a similar manner.

The sensitivity of the measurement as illustrated in Figs. 6 and 7 is of order 10^{-10} J/K at 3.4 K for a temperature oscillation of ~ 1 mK. For comparison, the heat capacity of 0.1 monolayer of adsorbed ^{4}He in the gas phase on one surface of the calorimeter is of order 5×10^{-10} J/K. Coverages of as little as 0.01 monolayer of ^{4}He have been detected.

Before exploring the heat capacity of adsorbates on metallic films deposited on the front surface of the calorimeter, we undertook a study of the heat capacity of submonolayers of ^{4}He adsorbed on bare, optically polished sapphire. This study is of practical importance to the operation of composite infrared bolometers that are similar in construction to this calorimeter. The added heat capacity of one adsorbed monolayer on such a bolometer has never been measured directly, although reductions in bolometer sensitivity have been observed upon exposure to small amounts of ^{4}He.[41]

The sapphire substrates are ultrasonically cleaned in electronic grade 1,1,1-trichloroethelyene, acetone and methanol prior to assembly of the calorimeter. After this treatment, the substrates are handled only on the edges with stainless steel tweezers that have been cleaned in the same manner. After assembly, the calorimeter is baked in air at 100 C for several hours to complete curing of the epoxy. The calorimeters are submerged in ^{4}He for calibration of the thermometers and then installed in the UHV system. After several days of pumping without bakeout, the base

pressure of this system is as low as 10^{-9} torr. Upon cooling of the radiation shields to 100 K and the cold finger to 1.5 K, the pressure near the calorimeter is less than 10^{-11} torr. Before measurements, the calorimeter is briefly warmed to slightly above room temperature to remove adsorbed contamination. This temperature was limited by the epoxy used to fabricate the calorimeter. No further surface preparation was used for these studies. It is probable that water is present on the surface. Adsorbed hydrocarbons are also possible.

At the beginning of each experiment, the heat capacity of the bare calorimeter is measured at a series of temperatures between 1.7 and 4.2 K. Then the front surface of the calorimeter is exposed to a beam of ^{4}He atoms from a room temperature effusion cell. The pressure in the effusion cell is monitored with an ionization gauge. Since the geometry of the cell and the distance to the calorimeter are known, the number of incident atoms per unit time is known. Exposures of 5 atoms per square angstrom of sapphire were typical. However, an undetermined fraction of the incident ^{4}He atoms adsorb on the sapphire under these circumstances, so the absolute coverage is unknown. After the exposure is complete, the heat capacity of the calorimeter plus adsorbates is measured at the same temperatures as before the dose. The heat capacity of the ^{4}He is obtained by subtraction.

The heat capacity of several coverages of ^{4}He on sapphire was measured. The data for three of these coverages are shown in Fig. 8. Since the absolute coverage is unknown, the units on the vertical axis are simply J/K for the adsorbed ^{4}He, which is spread over the 0.32 cm^2 surface

21

area of the front of the calorimeter below 3.3 K. Above 3.3 K, the heat capacity of the adsorbed ^{4}He decreases with increasing temperature. Measurements of the heat capacity at 2 K separated by brief ramps to higher temperatures demonstrated that desorption occurs above 3.3 K. The ^{4}He is entirely desorbed from the sapphire at 4.2 K. The measured heat capacity below 3.3 K can be interpreted as a superposition of two components. One component has heat capacity independent of coverage. The heat capacity of this component increases with temperature from 1.8 to 3.3 K. The second component is independent of temperature but increases with coverage.

A qualitative understanding of these results is possible despite the lack of a well characterized substrate. The ^{4}He states with the lowest free energy are laterally bound near defects and impurities on the sapphire surface. Higher energy states with lateral mobility exist over the rest of the surface. A low coverage of ^{4}He would occupy the lowest energy bound states first. Higher coverages of ^{4}He would occupy some mobile states as well as the bound states. The heat capacity of a low coverage of ^{4}He would increase with temperature due to excitation of atoms within bound states and promotion from bound states to mobile states. The heat capacity of a high coverage of ^{4}He would have the same contribution from the bound states as the low coverage, plus an additional temperature-independent component due to the mobile states. The decreases in heat capacity above 3.3 K occur due to desorption of the ^{4}He.

A more detailed explanation of these results would require knowledge of the distribution of binding energies presented by a partially

contaminated sapphire surface. Rather than continue studies of ^{4}He on sapphire, we have begun studies of ^{4}He on evaporated noble metal films. Preliminary measurements of ^{4}He adsorbed on evaporated Ag films in this apparatus have seen evidence for gas phase behavior over a wide range of coverages.[24]

IV Conclusion

This report describes the design, characterization, and operation of an instrument capable of measuring the heat capacities of submonolayers of adsorbed gas on a variety of evaporated substrates. The accuracy and sensitivity of the instrument have been demonstrated by measurements of the heat capacity of small samples of In near their superconducting transition. The ability to do heat capacity measurements on noble metal substrates is of great importance in the determination of the role of the substrate in the behavior of adsorbed systems. We plan to continue our studies of the heat capacity of monolayers of adsorbed ^{4}He and H$_2$ on evaporated noble metal films.

Acknowledgements

M.H.W. Chan, Y.P. Wang, J. Krim, J. Ma and R.B. Phelps. T.W. Kenny
gratefully acknowledges the support of an AT&T Bell labs fellowship

Figure Captions

Fig. 1) A schematic drawing of the calorimeters constructed for this project. The Cu leads are attached to the NiCr films and the Ge:Ga thermometers with conductive epoxy. One of the heaters is used to induce a temperature oscillation, and the other is used to regulate the temperature of the calorimeter.

Fig. 2) Plot of the product of the amplitude of the temperature oscillation of the calorimeter and the frequency of the oscillation as a function of the frequency of the osacillation. The plateau, which extends from 300 Hz to 1 kHz, indicates the range of operation of the calorimeter. The rolloff above 1 kHz is due to RC time constants which are associated with the heat sinks.

Fig. 3) The calorimeter mount and frame with the calorimeter in place. The calorimeter is constrained within the frame, which also serves as a mask for in-situ evaporation of clean surfaces. The mount is attached to the cold finger in the UHV system and can be cooled to 1.6 K during measurements.

Fig. 4) A cross-section of the cryostat and UHV system. The upper part includes storage canisters for the liquid nitrogen and pumped liquid ^{4}He. The lower half is an ion-pumped vacuum chamber, allowing surface preparation and heat capacity measurements at pressures as low as 10^{-12} torr. The evaporation source, effusion cell, and mass spectrometer are mounted on flanges at the level of the sample. Evaporation of fresh films, and dosing of the calorimeter with adsorbates takes place through a series

of holes in the radiation shields. One of the liquid nitrogen temperature shields can be rotated to prevent room temperature radiation from reaching the sample directly during measurements.

Fig. 5) A block diagram of the data acquisition system The ac heater bias is obtained from the reference channel of the PAR 5208 lock-in amplifier. The dc thermometer bias is obtained from a series of 9 V mercury batteries and a wire wound potentiometer. The amplitude of the induced voltage oscillation of the thermometer is measured by the PAR 5101 lock-in amplifier. The dc voltage of the thermometer is amplified by a PAR 113 preamplifier and then low-pass filtered to remove the ac components. The outputs are connected to the ADC channels of the computer and recorded. If the temperature of the thermometer drifts during the measurement, the regulation voltage , which is derived from the DAC channels of the computer, is fed back to counteract the drifts.

Fig. 6) The hysteresis in the superconducting transition of a 25 μg In sample on the calorimeter. Such hysteresis is typical of the expected supercooling in the presence of a small applied magnetic field.

Fig. 7) The heat capacity of a second In sample attached in a similar manner to that in Fig. 5. In this case, supercooling is not observed, probably because of a greater concentration of defects which can nucleate the formation of the superconducting phase.

Fig. 8) The heat capacity of three coverages of ^{4}He on sapphire. The heat capacity of the bare calorimeter has already been subtracted. The
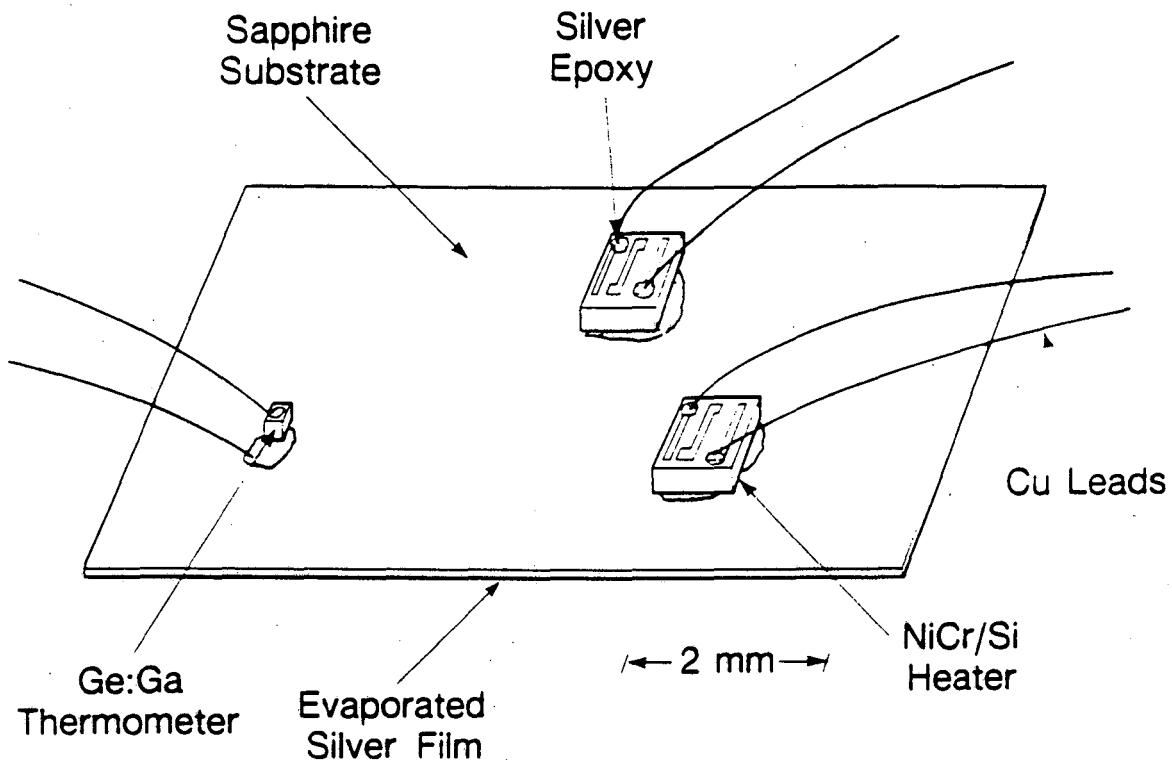
temperature dependence above 3.3 K is dominated by desorption of the adsorbed ^{4}He.

* Present address : Jet Propulsion Laboratory, 4800 Oak Grove Dr. Pasadena, CA 91109

[1] M. Bretz, J.G. Dash, Phys. Rev. Lett. 26, 963 (1971).

[2] M. Bretz et al., Phys. Rev. A 8, 1589 (1973).

[3] Q.M. Zhang, H.K. Kim, M.H.W. Chan, Phys. Rev. B 32, 1820 (1985).

[4] A.D. Migone, Z.R. Li, M.H.W. Chan, Phys. Rev. Lett. 53, 810 (1984).

[5] J. Krim, J.P. Coulomb, J. Bouzidi, Phys. Rev. Lett. 58, 583 (1987).

[6] F.C. Motteler, J.G. Dash, Phys. Rev. B 31, 346 (1985).

[7] J.M. Kosterlitz, D.J. Thouless, in Progress in Low Temperature Physics, Vol VII-B, edited by Brewer, D.F. (North-Holland, Amsterdam), p. 373 (1978).

[8] D.R. Nelson, B.I. Halperin, Phys. Rev. B 19, 2457 (1979).

[9] A.P. Young, Phys. Rev. B 19, 1855 (1979).

[10] T.V. Ramakrishnan, Phys. Rev. Lett. 48, 1114 (1982).

[11] S.T. Chui, Phys. Rev. B 28, 178 (1983).

[12] H. Kleinert, Phys. Lett. A 95, 381 (1983).

[13] K.J. Strandburg, Rev. Mod. Phys. 60, 161 (1988).

[14] G.P. Boato et al., Surf. Sci. 80, 518 (1979).

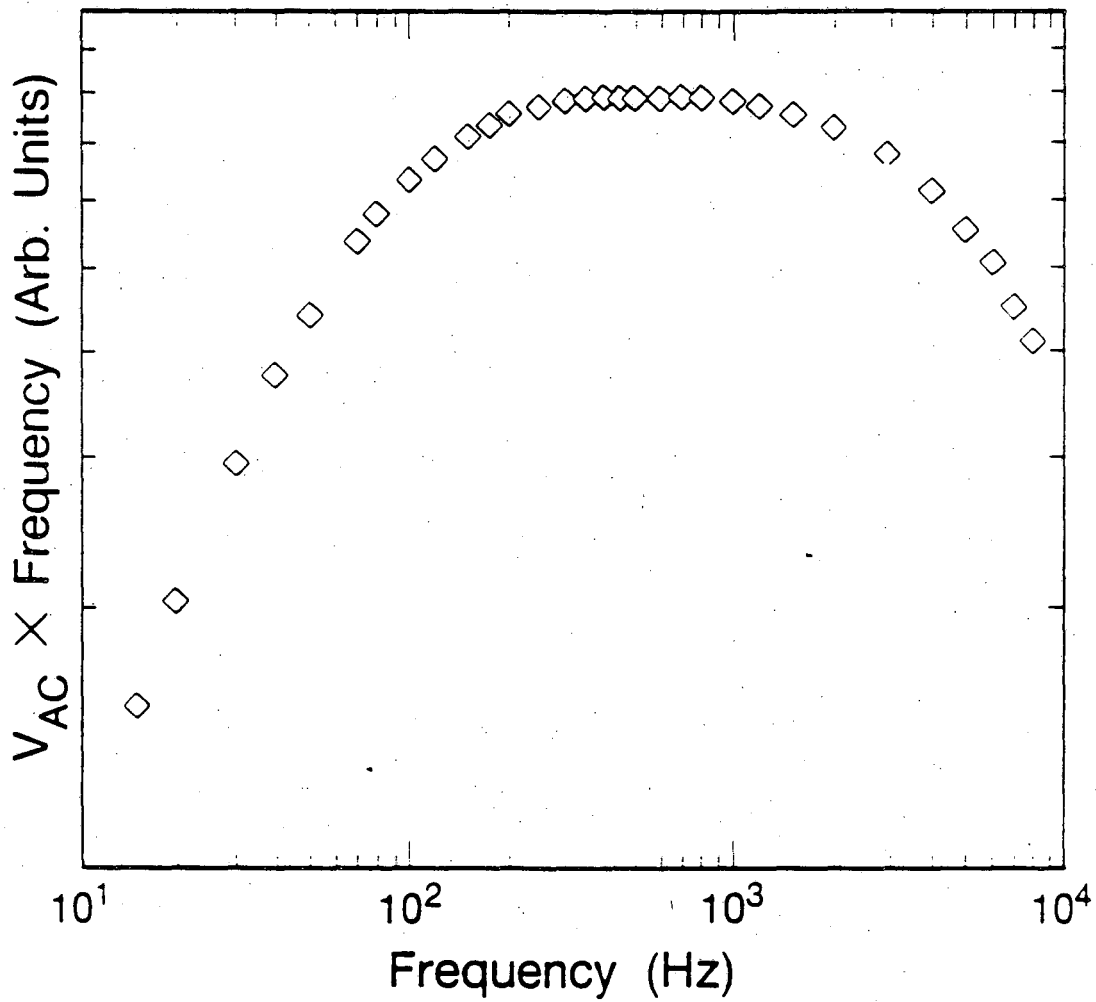[15] G.D. Derry et al., Surf. Sci. 87, 629 (1979).

[16] M.W. Cole et al., Rev. Mod. Phys. $\underline{53}$, 199 (1981).

[17] W.E. Carlos, M.W. Cole, Phys. Rev. B $\underline{21}$, 3713 (1980).

[18] C. Schwartz, M.W. Cole, Phys. Rev. B $\underline{34}$, 1250 (1986).

[19] N. Greiser et al, Phys. Rev. Lett. $\underline{59}$, 1706 (1987).

[20] J.K. Gimzewski et al, Phys. Rev. Lett. $\underline{55}$, 951 (1985).

[21] P.F. Sullivan, G. Seidel, Phys. Rev. $\underline{173}$, 679 (1968).

[22] R.A. Smith, F.E. Jones, R.P. Chasmar, The Detection and Measurement of Infra-red Radiation, Oxford University Press, London (1968) P. 185

[23] Ibid p. 212.

[24] T.W. Kenny, P.L. Richards, Bull. Am. Phys. Soc. $\underline{33}$, 264 (1988).

[25] A.E. Lange et al., Int. J. IR+MM Waves $\underline{4}$, 689 (1983).

[26] MSTF-3-S-N-1K, Mini-Systems, Inc., North Attleboro, MA.

[27] Epo-Tek H20E, Epoxy Technology Inc., Billerica, Ma.

[28] E.E.Haller, IR Phys. $\underline{25}$, 257 (1985).

[29] T.W. Kenny et al, Phys. Rev. B $\underline{39}$, 8476 (1989).

[30] D. McCammon et al, J. Appl. Phys $\underline{56}$, 1263 (1985).

[31] M. T. Loponen et al, Phys. Rev. B $\underline{25}$, 1161 (1982).

[32] Stychast 2850-FT, Emerson & Cuming, Inc., Canton, Mass 02021.

[33] W.R. McGrath and P.L. Richards, Rev. Sci. Instr. 53, 709 (1982).

[34] PAR 5208, Princeton Applied Research Inc., Princeton, NJ.

[35] PAR 113, Princeton Applied Research Inc., Princeton, NJ.

[36] PAR 5101, Princeton Applied Research Inc., Princeton, NJ.

[37] DT2785-DI/5716-B-PGL, Data Translation Inc., Marlboro, MA.

[38] T.W. Kenny, P.L. Richards, to be published.

[39] E.A. Lynton, Superconductivity, Methuen & Co. LTD, London p. 69 (1969).

[40] T.E. Faber, Proc. Roy. Soc. (London) A241, 531 (1957).

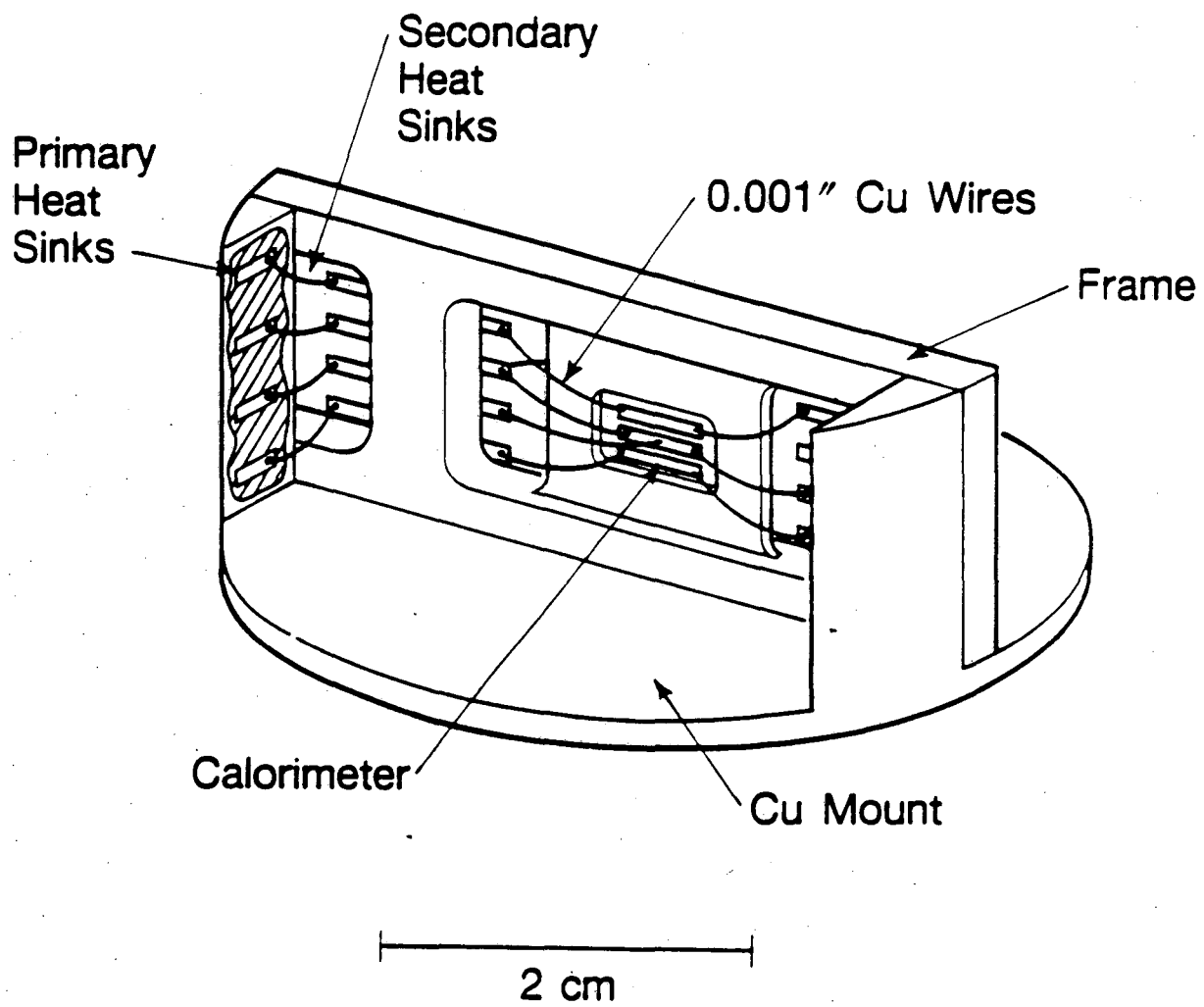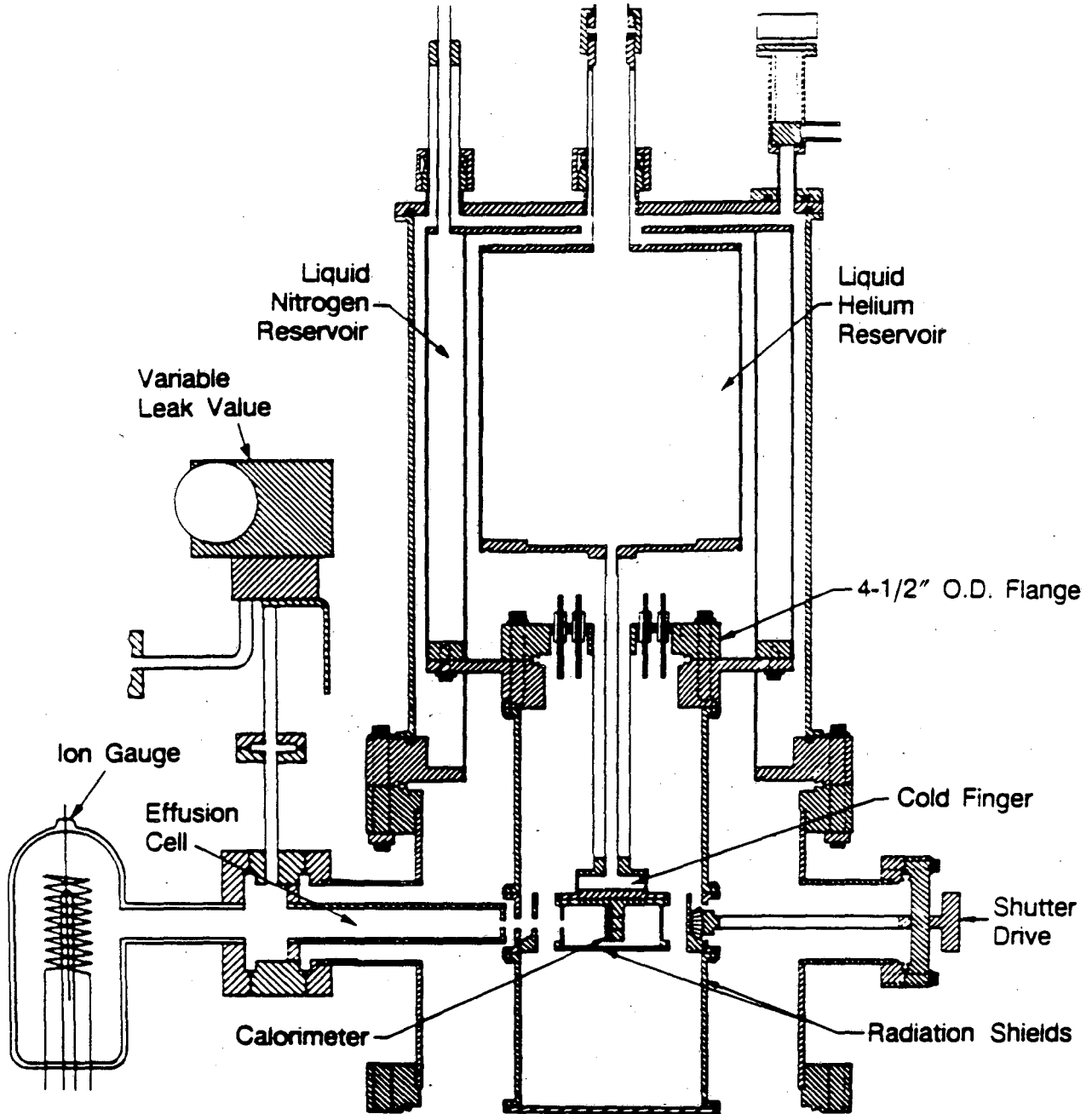[41] A.E. Lange, S.H. Moseley, private communication.

Sapphire Substrate

Silver Epoxy

Cu Leads

Ge:Ga Thermometer

Evaporated Silver Film

NiCr/Si Heater

$\leftarrow$ 2 mm $\rightarrow$

FIGURE 1

FIGURE 2

XBL 893-5062

32

Secondary Heat Sinks

Primary Heat Sinks

0.001″ Cu Wires

Frame

Calorimeter

Cu Mount

2 cm

XBL 8810-7636

FIGURE 3

33

Liquid Nitrogen Reservoir

Variable Leak Value

Ion Gauge

Effusion Cell

Calorimeter

Liquid Helium Reservoir

4-1/2″ O.D. Flange

Cold Finger

Shutter Drive

Radiation Shields

XBL 772-7512C

FIGURE 4

34

Calorimeter 571 KΩ Computer

Bias

V_{DC}

Thermometer

PAR 113

AC Heater

S
PAR
5101
R

V_{AC}

S
PAR
5208
R

V_H

DAC$_1$

Regulation
Heater

10 kΩ

DAC$_2$

100 Ω

XBL 8810-7637

FIGURE 5

35

FIGURE 6

XBL 8810-7633

36

XBL 8810-7634

FIGURE 7

Heat Capacity (J/K × 10^{-10}) vs Temperature (K)

XBL 8810-7666

FIGURE 8

38